Asymmetric Supply of a Dual Three-Phase PMSM through a Hybrid Energy Storage System in Marine Electric Propulsion Systems

Alessandro Serpi, Mario Porru, Andrea Turno
Department of Electrical and Electronic Engineering
University of Cagliari
Cagliari, Italy

Fabio Tinazzi, Marco Pastura, Mauro Zigliotto
Department of Management and Engineering
University of Padova
Vicenza, Italy

***Abstract*—This paper proposes a novel electric propulsion system architecture for marine applications. This consists of a Hybrid Energy Storage System (HESS) supplying a Dual Three-Phase Permanent Magnet Synchronous Machine (DTP-PMSM), which is connected to a marine propeller through a gearbox so that it acts as the propulsion motor of the vessel. The HESS is made up of a battery pack and a supercapacitor module, each of which supplies one of the two DTP-PMSM three-phase windings through suitable DC/DC and DC/AC converters. Vessel speed can be regulated through suitable DTP-PMSM speed and current control loops. Additionally, torque/power demand can be split asymmetrically between the two DTP-PMSM windings according to power and/or energy capability of each HESS unit. The proposed configuration is validated through numerical simulations, which highlight the effectiveness of both HESS energy management and DTP-PMSM control systems.**

***Keywords*—Batteries, Electric propulsion systems, Energy management, Permanent magnet synchronous machines, Supercapacitors**

I. Introduction

The ever-increasing awareness about the impact of harmful emissions on climate changes, as well as their effects on planet and human health, continuously urge technological actions to hand over a climate-neutral world to next generations. To contribute to such a challenging target, the International Maritime Organization (IMO) and national authorities aim at limiting emissions of waterborne transports. Electrification is a viable solution to tackle this environmental challenge, and vessels with frequent port calls represent a key technology enabler to contribute towards such a paradigm shift in marine applications [1].

Hybrid vessels configurations, i.e. a combination of combustion engines and electric motors, increase the overall efficiency, but also increase costs and complexity, thus the energy management system must ensure that engines operate close to their optimum to achieve fuel saving [2], [3], [4]. Although hybridization increases the overall system efficiency, it does not prevent greenhouse gas emission and acoustic noise as a full electric solution can do. At this aim, the development of novel power electronic converters and electric motors for marine applications has been increasing considerably in the last decade [5], [6]. Full electric solutions require electric machines of considerable rated power. Furthermore, redundancy is of paramount importance. These are some of the motivations for the adoption of multiphase motors in marine Electric Propulsion Systems (EPSs) [7]. Among the several multiphase machine configuration, the Dual Three-Phase Permanent Magnet Synchronous Machine (DTP-PMSM) offers a good compromise between redundancy and complexity [8].

A potential advantage that multiphase electric motors bring along is the possibility to feed each three-phase winding with a different energy source, thus enabling the employment of a Hybrid Energy Storage System (HESS). This is a very attractive possibility, since the mixture of electric energy sources appears as an effective choice for marine EPSs [9]. However, the challenge of a correct utilization of each energy source calls for an asymmetric exploitation of the two or more three-phase windings. In other words, it is necessary to achieve an unbalanced power, torque and current distribution among the three-phase windings [10].

In this scenario, a novel EPS architecture for a full-electric tugboat is presented in this paper. The proposed configuration consists of a DTP-PMSM connected to a marine propeller through a gearbox. The two DTP-PMSM three-phase windings are supplied by a battery pack and a supercapacitor module; such an asymmetric supply represents the distinctive feature of the proposed solution, which requires an unbalanced torque and current distribution among the two windings to enable an appropriate energy management and exploitation of the different energy storage units onboard. In this regard, a frequency-based energy management system is proposed, together with a suitable PI-based control system for regulating tugboat speed, DTP-PMSM speed and currents. The effectiveness of the proposed EPS architecture is verified through numerical simulations, which reveal the good performance achieved in terms of both energy management and speed/current control.

II. System overview and modelling

The EPS architecture proposed in this paper can be represented as in Fig. 1. Particularly, the key device is the DTP-PMSM, whose windings are supplied by a Battery Pack (BP) and a Supercapacitor Module (SM) through appropriate DC/DC and DC/AC converters. The DTP-PMSM shaft is connected through a gearbox to a marine propeller, which develops the thrust force to move the vessel in accordance with its speed or power requirements. Modelling of both DTP-PMSM and marine propeller are reported in the following subsections.

This is the Author's accepted manuscript version of the following contribution:
A. Serpi, M. Porru, A. Turno, F. Tinazzi, M. Pastura and M. Zigliotto, "Asymmetric Supply of a Dual Three-Phase PMSM through a Hybrid Energy Storage System in Marine Electric Propulsion Systems," 2024 IEEE Vehicle Power and Propulsion Conference (VPPC), Washington, DC, USA, 2024, pp. 1-6, doi: 10.1109/VPPC63154.2024.10755331

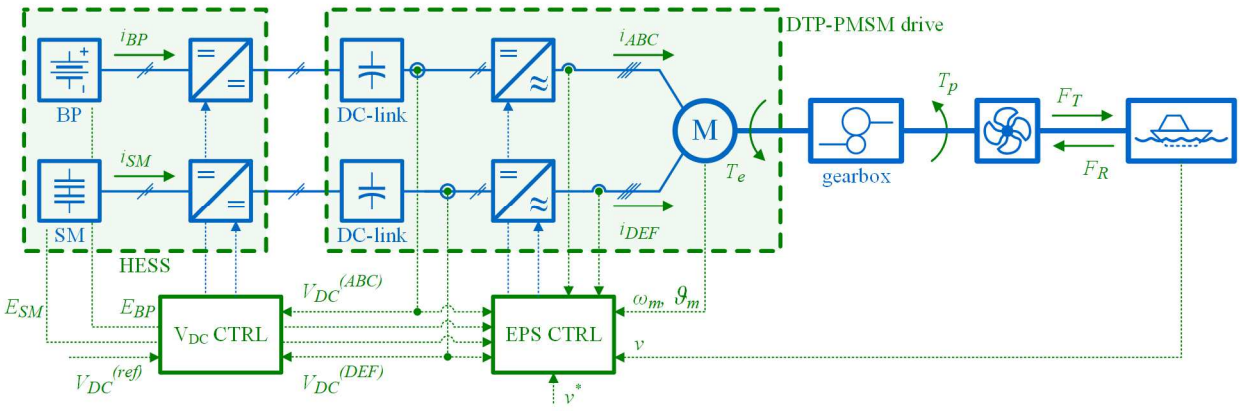

Fig. 1. Overview of the proposed EPS architecture.

A. DTP-PMSM

The phase voltage equations of a DTP-PMSM can be expressed as

$$\left[v_{ph}\right]=r\left[i_{ph}\right]+\frac{d\left[\lambda_{ph}\right]}{dt} \tag{1}$$

where r is the phase winding resistance, while $[v_{ph}]$, $[i_{ph}]$, and $[\lambda_{ph}]$ denote the phase voltage, current, and magnetic flux linkage vectors:

$$\left[x_{ph}\right]=\left[x_A,x_B,x_C,x_D,x_E,x_F\right]^T,\quad x\in\{v,i,\lambda\}. \tag{2}$$

The magnetic flux linkage vector can be further expressed as

$$\left[\lambda_{ph}\right]=\left[L\right]\left[i_{ph}\right]+\left[\lambda_{m,ph}\right] \tag{3}$$

in which $[L]$ is the inductance matrix and $[\lambda_{m,ph}]$ is the magnetic flux linkage vector component due to PM only. Assuming a magnetically isotropic DTP-PMSM structure and its three-phase winding electrically displaced by 30 deg, $[\lambda_{m,ph}]$ can be further expressed as

$$\lambda_{m,x}=\Lambda\cos\left(\vartheta-\delta_x\right),\quad x\in\{A,B,C,D,E,F\} \tag{4}$$

where Λ denotes the equivalent magnetic flux linkage magnitude due to PM, ϑ is the electric rotor position, while

$$\left[\delta_{ph}\right]=\left[0,\tfrac{2}{3}\pi,\tfrac{4}{3}\pi,\tfrac{1}{6}\pi,\tfrac{5}{6}\pi,\tfrac{3}{2}\pi\right]^T. \tag{5}$$

Given (1)-(5), the DTP-PMSM model can be more usefully expressed in terms of space vectors in the stationary reference frame (αβxy0z) by applying the following expressions:

$$\begin{aligned}
x_{\alpha\beta}&=\tfrac{2}{3}\left(x_A+x_Be^{j\frac{2}{3}\pi}+x_Ce^{j\frac{4}{3}\pi}+x_De^{j\frac{1}{6}\pi}+x_Ee^{j\frac{5}{6}\pi}+x_Fe^{j\frac{3}{2}\pi}\right)\\
x_{xy}&=\tfrac{2}{3}\left(x_A+x_Be^{j\frac{4}{3}\pi}+x_Ce^{j\frac{2}{3}\pi}+x_De^{j\frac{5}{6}\pi}+x_Ee^{j\frac{1}{6}\pi}+x_Fe^{j\frac{3}{2}\pi}\right)\\
x_{0z}&=\tfrac{1}{3}\left(x_A+x_B+x_C+\left(x_D+x_E+x_F\right)e^{j\frac{1}{2}\pi}\right).
\end{aligned} \tag{6}$$

Hence, by substituting (3) in (1), and by applying (6) to the resulting equations are

$$\begin{aligned}
v_{\alpha\beta}&=r\,i_{\alpha\beta}+L_s\frac{di_{\alpha\beta}}{dt}+2j\omega\Lambda e^{j\vartheta}\\
v_{xy}&=r\,i_{xy}+L_0\frac{di_{xy}}{dt},\quad v_{0z}=r\,i_{0z}+L_0\frac{di_{0z}}{dt}
\end{aligned} \tag{7}$$

in which L_s and L_0 denote the synchronous and the zero-sequence inductance, respectively, while ω is the electric rotor speed, proportional to the mechanical speed (ω_m) through the number of poles pairs (p). Hence, (7) reveals that PM does not have any effect on xy and 0z reference frames, which, therefore, do not account for any torque contribution. Consequently, moving from the αβ to the synchronous reference frame (dq+) by the Park transformation leads to

$$v_{dq+}=\left(r+j\omega L_s\right)i_{dq+}+L_s\frac{di_{dq+}}{dt}+2j\omega\Lambda. \tag{8}$$

Considering the power balance and denoting by $^-$ the complex conjugate operator, the electromagnetic power and torque can be expressed as

$$P_m=\frac{3}{4}\Re\left\{2j\omega\Lambda\bar{i}_{dq+}\right\}=\frac{3}{2}\omega\Lambda i_{q+},\quad T_e=\frac{P_m}{\omega_m}=\frac{3}{2}p\Lambda i_{q+}. \tag{9}$$

Given (7), although xy current components do not contribute to the overall electromagnetic torque and power, they affect the contribution that each DTP-PMSM winding gives to them. In this regard, consider two three-phase current vectors characterized by the same angular displacement (φ) but different magnitudes (I_{ABC} and I_{DEF}):

$$i_h=I_{ABC}\cos\left(\vartheta-\varphi-\delta_h\right),\quad h\in\{A,B,C\} \tag{10}$$

$$i_k=I_{DEF}\cos\left(\vartheta-\varphi-\delta_k\right),\quad k\in\{D,E,F\}. \tag{11}$$

Substituting (10)-(11) in (6) and neglecting 0z components yields

$$i_{\alpha\beta}=\left(I_{ABC}+I_{DEF}\right)e^{j(\vartheta-\varphi)},\quad i_{xy}=\left(I_{ABC}-I_{DEF}\right)e^{-j(\vartheta-\varphi)} \tag{12}$$

Therefore, (12) reveals that any magnitude unbalance between DTP-PMSM winding currents do not affect αβ current components as long as their sum is kept constant, but it always produces a counter-rotating current space vector in the xy

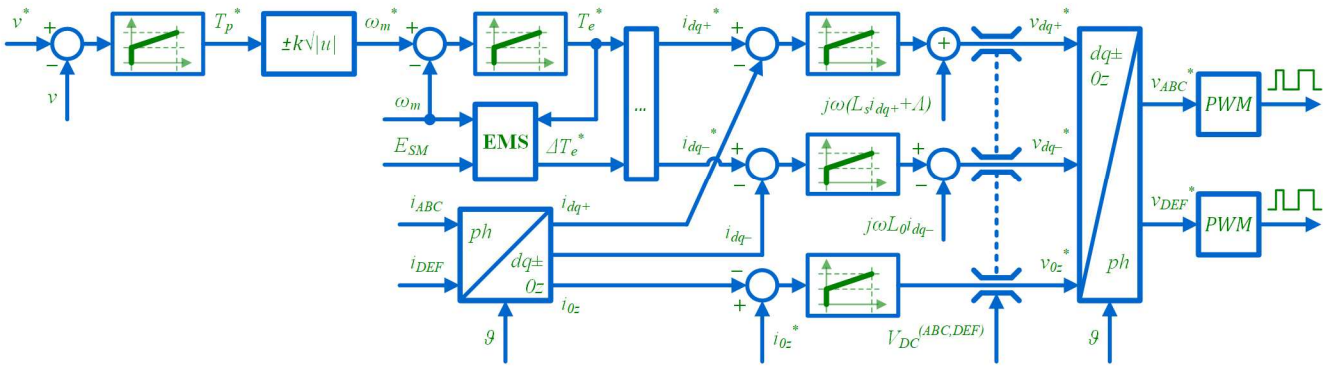

Fig. 2. Exploded view of the block "EPS CTRL" shown in Fig. 1.

reference frame. Consequently, the latter can be usefully employed to prevent or impose a current/torque unbalance, such as the case considered in this paper. Particularly, moving from the αβ and xy to the dq+ and dq– reference frames, (12) becomes:

$$i_{dq+} = \left(I_{ABC} + I_{DEF}\right) e^{-j\varphi}, \quad i_{dq-} = \left(I_{ABC} - I_{DEF}\right) e^{j\varphi} \tag{13}$$

while (8) can be joined by:

$$v_{dq-} = \left(r - j\omega L_0\right) i_{dq-} + L_0 \frac{di_{dq-}}{dt} \tag{14}$$

which is achieved from (7) by moving from the xy to the dq– reference frame. Similarly, given (13), (9) can come along with the following expressions:

$$\Delta P_m = \frac{3}{2}\omega \Lambda i_{q-}, \quad \Delta T_e = \frac{3}{2} p \Lambda i_{q-} \tag{15}$$

which quantifies the additional electromagnetic power/torque provided by the winding DEF compared to ABC (positive values). As a result, constant q+ and q– current components can be imposed in accordance with DTP-PMSM cumulative and differential power/torque demands.

In conclusion, the torque equation at the DTP-PMSM shaft can be expressed as:

$$T_e = J\frac{d\omega_m}{dt} + D\omega_m + T_L \tag{16}$$

in which J and D represent the inertia and the damping coefficient, respectively, while T_L is the propeller load torque.

B. Marine propeller

A fixed-pitch propeller has been considered in this study, whose torque T_p and thrust force F_p can be expressed as [11]

$$T_p = \sigma_\omega k_T \rho D_p^5 \left(\frac{\omega_p}{2\pi}\right)^2, \quad F_P = k_F \rho D_p^4 \left(\frac{\omega_p}{2\pi}\right)^2 = \frac{k_F}{k_T}\frac{T_p}{D_P} \tag{17}$$

where σ_ω is the sign of the propeller speed (ω_p), k_T and k_F are the torque and the thrust coefficient, respectively, ρ is the water mass density, and D_p is the propeller diameter. Propeller torque and speed depend on DTP-PMSM speed and load torque through the gear ratio τ as

$$T_L = \frac{T_p}{\tau}, \quad \omega_p = \frac{\omega_m}{\tau} \tag{18}$$

C. Vessel

Vessel modelling consists of its motion equation only:

$$F_p = M\frac{dv}{dt} + F_r, \quad F_r = \sigma_v f \frac{1}{2}\rho S_v v^2 \tag{19}$$

in which M is the vessel mass, while F_r is the resistance force. In particular, assuming no sea current speed, F_r depends on ρ, f, which is a dimensional-less coefficient depending on the Froude's number, and the vessel wetted area (S_v) [11].

III. Control System Design

The overview of the overall EPS control system is shown in Fig. 2. This consists of several cascade PI-based control loops that aim at regulating vessel speed, DTP-PMSM speed and currents appropriately, by taking into account also the torque unbalance eventually imposed by the EMS.

A. Vessel control

The outer control loop aims at regulating the vessel speed in accordance with (19). Consequently, due to the nonlinear relationship between F_r and v, the former has been approximated as

$$\tilde{F}_r = \left(\frac{1}{2}\bar{f}\rho S_v v_n\right)v - \left(\frac{1}{12}\bar{f}\rho S_v v_n^2\right), \quad v \in [0, v_n] \tag{20}$$

in which $\bar{f}$ is the average value of f within the considered vessel speed range, and v_n is the vessel rated speed. Consequently, by replacing F_r with $\tilde{F}_r$ in (19), and given (17), the vessel speed can be regulated successfully by means of a PI regulator, which determines the reference propeller torque T_p^* in accordance with the desired dynamic performance. Once T_p^* has been defined, the corresponding DTP-PMSM reference speed can be computed easily based on (17)-(18).

B. DTP-PMSM control

The DTP-PMSM control system consists of an outer speed loop and three inner current control loops, as still shown in Fig. 2. Particularly, the speed loop can be designed based on (16)-(18), but replacing T_p with the following approximation:

$$\tilde{T}_p = \left(k_T \rho \frac{D_p^5}{4\pi^2}\frac{\omega_{m,n}}{\tau^2}\right)\omega_m - \left(k_T \rho \frac{D_p^5}{24\pi^2}\frac{\omega_{m,n}^2}{\tau^2}\right), \quad \omega_m \in [0, \omega_{m,n}] \tag{21}$$

where $\omega_{m,n}$ is the DTP-PMSM rated speed. Therefore, a PI

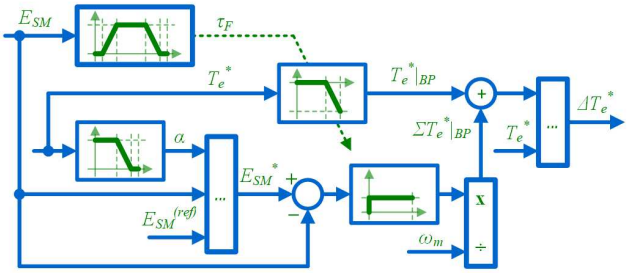

Fig. 3. The proposed EMS.

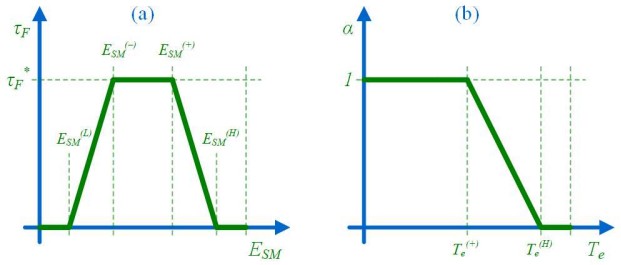

Fig. 4. The filter time constant τ_F (a) and the α coefficient (b) graphs.

regulator similar to that employed for vessel speed control can be designed, which computes the reference torque T_e^* to be provided by the DTP-PMSM. The latter is then processed by the EMS, which determines the required torque unbalance ΔT_e^* depending on DTP-PMSM speed and SM energy content (E_{SM}), as detailed in the following section.

Once both T_e^* and ΔT_e^* have been achieved, they are combined to each other to determine positive- and negative-sequence reference q current components in accordance with (9) and (15). In addition, reference d and 0z current components can be set to zero as they do not contribute to T_e, and there is no need for flux-weakening operation. As a result, the reference dq and 0z current profiles can be tracked by suitable PI regulators, which are designed in the dq+, dq–, and 0z reference frames based on (8), (14), and (7), respectively. As a result, all the reference voltage in the dq+, dq–, and 0z reference frames can be achieved, based on which the corresponding reference phase voltages can be achieved through Park and/or Clarke transformation. These reference voltages feed two PWM modulators, each of which synthesizes the command signals for the corresponding DC/AC converter supplying one of the two DTP-PMSM windings.

IV. Energy Management

The proposed EMS architecture has been developed based on two main considerations. First, SM should support BP over fast torque variations. Second, SM energy content is much smaller than BP, so SM charge reinstatement must be considered over medium-long time ranges. Both these requirements are accounted by the block control scheme depicted in Fig. 3, which consists of two main branches.

Considering the upper branch first, the reference torque signal T_e^* is processed by a low-pass filter to achieve a smoother profile that should be handle by BP winding (ABC) on its own ($T_e^*|_{BP}$). In this regard, the filter time constant τ_F is varied with the SM energy content (E_{SM}), as shown in Fig. 4a. In particular, when E_{SM} overcomes two thresholds in approaching its maximum or minimum value, τ_F is gradually reduced to make $T_e^*|_{BP}$ less different from T_e^*. This means that SM support is gradually reduced so that T_e^* can be always assured, at least by BP only.

Considering the lower branch, it consists mainly of an SM energy loop, which employs a P regulator to achieve the additional torque required from BP winding ($\Sigma T_e^*|_{BP}$) to reinstate E_{SM} to E_{SM}^*. The latter generally equals a suitable intermediate value ($E_{SM}^{(ref)}$). However, when T_e^* is relatively large, E_{SM}^* is computed as

$$E_{SM}^* = \alpha E_{SM}^{(ref)} + (1-\alpha) E_{SM}, \quad \alpha \in [0,1] \tag{22}$$

in which α varies in accordance with Fig. 4b. Consequently, E_{SM}^* equals E_{SM} when T_e^* is approaching its rated value; this means that SM charging/discharging requirements are neglected when the torque demand is relatively high to avoid any BP overloading.

In conclusion, the sum of $T_e^*|_{BP}$ with $\Sigma T_e^*|_{BP}$ concurs with T_e^* to achieve the required torque unbalance ΔT_e^*, which is the only final output of the proposed EMS.

V. Simulation Results

The effectiveness of the proposed EPS configuration has been verified through simulations, which have been carried out in MATLAB-Simulink by referring to the scheme shown in Fig. 1, and to the parameters resumed in Table I and Table II. In particular, simulation parameters were defined based on similar-size vessel examples [11], [12]. For the sake of completeness, the data were supplemented and validated also with reference to existing electric tugboats, such as RSD Tug 2513 produced by Damen, and Zeetug produced by Navtek [13], [14]. Regarding the proposed EMS shown in Fig. 3, τ_F, E_{SM}, and T_e thresholds are setup with reference to their rated values, as summarized in Table III.

A reference tugboat speed profile is then imposed (Fig. 5) in accordance with a possible realistic scenario. In this regard, it is

TABLE I. Tugboat, Vessel, and Propeller Parameters

Parameter	Unit	Value
Tugboat & Assisted vessel		
M_{tug}	tons	600
L_{tug}	m	27.8
$S_{v,tug}$	m^2	392
$V_{tug,nom}$ @ transit mode	m/s (kts)	7.716 (15)
$V_{tug,nom}$ @ assist mode	m/s (kts)	2.058 (4)
M_{ves}	tons	100410
L_{ves}	m	246
$S_{v,ves}$	m^2	12339
P	kg/m^3	1000
v_w	m/s	0
Marine propeller		
$W_{p,nom}$	rpm	200
D_p	m	3
k_T	-	0.0347
k_F	-	0.1483
τ	-	5

TABLE II. EPS PARAMETERS

Parameter	Unit	Value
DTP-PMSM		
$P_{m,nom}$	MW	2.101
$T_{e,nom}$	kNm	20
I_{nom} (for each three-phase winding)	A	327.4
$\omega_{m,nom}$	rpm	1000
V_{nom}	kV	4.436
p	-	3
r	mΩ	20.6
L	mH	2.5
M	mH	0.8
Λ	Wb	6.788
δ	deg	30
DC-link, BP and SM		
$V_{DC,nom}$	*kV*	*5*
$P_{BP,nom}$	*MW*	*2.2*
$E_{BP,nom}$	*MWh*	*2*
$V_{BP,nom}$	*V*	*800*
$P_{SM,nom}$	*MW*	*2.2*
$E_{SM,nom}$	*MWh*	*0.07*
$V_{SM,nom}$	*V*	*800*

TABLE III. EMS PARAMETERS

Parameter	Unit	Value
τ_F	s	120
$E_{SM}^{(L)}$	pu	0.1
$E_{SM}^{(-)}$	pu	0.4
$E_{SM}^{(+)}$	pu	0.6
$E_{SM}^{(H)}$	pu	0.9
$T_e^{(+)}$	pu	0.8
$T_e^{(-)}$	pu	0.6

worth noting that, although simulation time is expressed in seconds, a suitable time scaling factor has been introduced. Consequently, mass and inertia coefficients have been modified so that seconds in simulations correspond to minutes, thus giving a more realistic representation of a tugboat operating scenario. The τ_F value has been reduced as well in accordance with the time scaling factor previously mentioned. The tugboat speed profile consists of three main stages. In the first stage (0-30 s), the tugboat is in transit operation, i.e. it navigates and approaches the vessel to tug. Assist mode then occurs in the second stage (30-120 s), when the tugboat pulls or pushes the vessel requiring assistance. Subsequently, the tugboat is assumed to go back to its docking place (120-165 s).

Simulation results are depicted in Fig. 6 and Fig. 7. Focusing on Fig. 6 at first, it can be seen that the reference tugboat speed profile is almost perfectly tracked up to 30 s, by requiring relatively small DTP-PMSM torque and speed values. After this, the tugboat is connected to the assisted vessel, which is then towed up to approximately 120 s; during this operating mode, DTP-PMSM torque and speed demands are significant, up to their rated values, while reference tugboat speed profile is tracked less accurately, but still acceptably, mainly due to the huge mass of the assisted vessel. An almost perfect tugboat reference speed tracking is recovered after the assisted vessel has been unhooked (~120 sec) and, thus, when the tugboat navigates on its own.

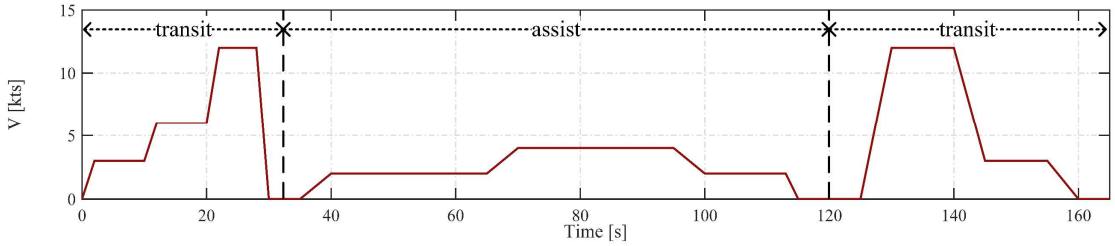

Fig. 5. Tugboat reference speed and operating modes.

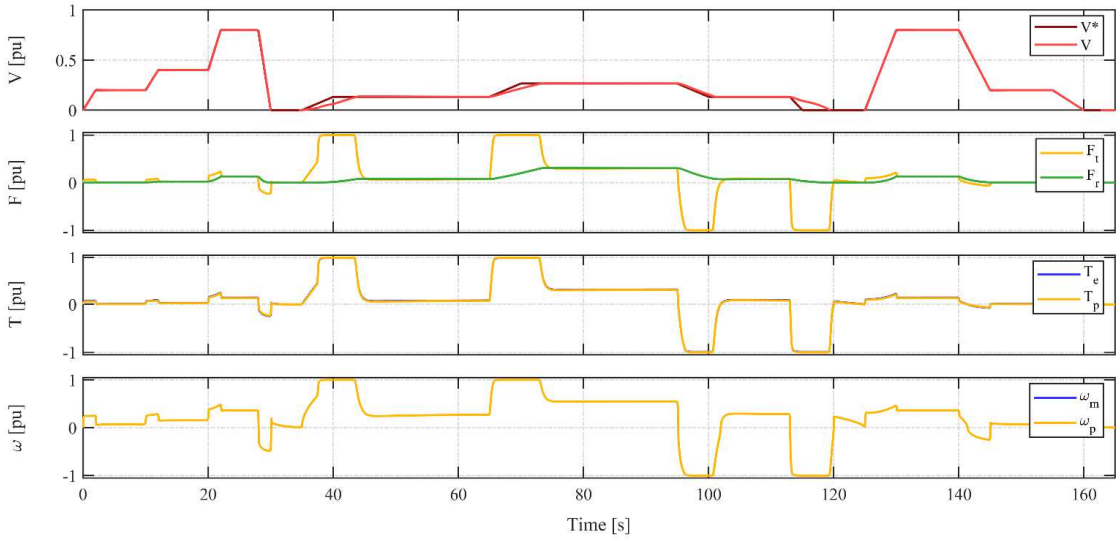

Fig. 6. Tugboat speed, thurst force, propeller and DTP-PMSM torque and speed profiles achieved in simulations.

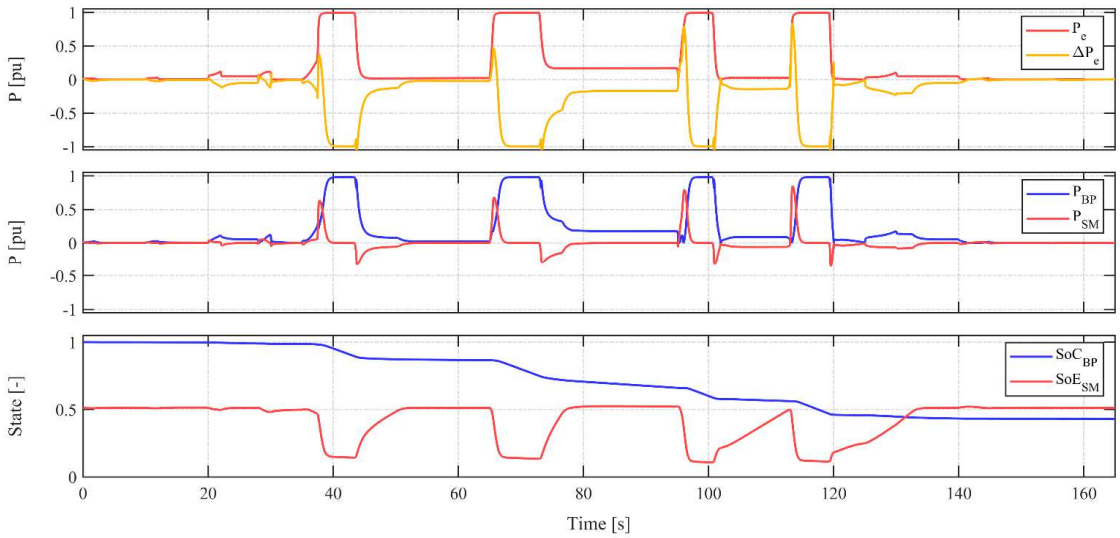

Fig. 7. Cumulative and differential DTP-PMSM electromagnetic power, BP and SM power demands and energy content achieved in simulations.

Considering DTP-PMSM, BP, and SM power demands (Fig. 7), it can be seen that marginal unbalances occur when the tugboat navigates freely due to the very low power required during these operating conditions. Differently, when the tugboat is connected to the assisted vessel and has to accelerate/decelerate, the DTP-PMSM rated power is suddenly required: this is supplied by SM first and, then, by BP. When the required speed is achieved, DTP-PMSM power demand decreases, and BP can recharge SM gradually without any overloading, thus confirming the effectiveness of the proposed energy management and control approach.

VI. Conclusion

A novel electric propulsion system architecture for a full-electric tugboat has been presented in this paper. This consists of a Dual Three-Phase Permanent Magnet Synchronous Machine (DTP-PMSM), whose three-phase windings are supplied by a Battery Pack (BP) and a Supercapacitor Module (SM). A suitable energy management system is proposed, which resorts to torque unbalance between the two DTP-PMSM windings to regulate the energy flow from/to the two different energy storage units appropriately. Simulation results highlight the effectiveness of the proposed configuration, especially in terms of tugboat speed control and SM exploitation during dynamic operations. Future works will address different energy storage system combinations, as well as a joint DC-link for both three-phase systems. A detailed performance assessment will be carried out as well, by considering a conventional three-phase single motor configuration for comparison purposes.

References

[1] Y. Ning, L. Wang, X. Yu, and J. Li, 'Recent development in the decarbonization of marine and offshore engineering systems', *Ocean Eng.*, vol. 280, p. 114883, Jul. 2023, doi: 10.1016/j.oceaneng.2023.114883.

[2] B. A. Kumar, R. Selvaraj, K. Desingu, T. R. Chelliah, and R. S. Upadhyayula, 'A Coordinated Control Strategy for a Diesel-Electric Tugboat System for Improved Fuel Economy', *IEEE Trans. Ind. Appl.*, vol. 56, no. 5, pp. 5439–5451, Sep. 2020, doi: 10.1109/TIA.2020.3010779.

[3] L. W. Y. Chua, T. Tjahjowidodo, G. G. L. Seet, and R. Chan, 'Implementation of Optimization-Based Power Management for All-Electric Hybrid Vessels', *IEEE Access*, vol. 6, pp. 74339–74354, 2018, doi: 10.1109/ACCESS.2018.2883324.

[4] L. W. Y. Chua, T. Tjahjowidodo, G. S. G. Lee, R. Chan, and A. K. Adnanes, 'Equivalent Consumption Minimization Strategy for hybrid all-electric tugboats to optimize fuel savings', in *Proc. of American Control Conference 2016 (ACC 2016)*, Boston, MA, USA: IEEE, Jul. 2016, pp. 6803–6808. doi: 10.1109/ACC.2016.7526743.

[5] H. Mahdi, B. Hoff, and T. Østrem, 'A Review of Power Converters for Ships Electrification', *IEEE Trans. Power Electron.*, vol. 38, no. 4, pp. 4680–4697, Apr. 2023, doi: 10.1109/TPEL.2022.3227398.

[6] E. Skjong, R. Volden, E. Rødskar, M. Molinas, T. A. Johansen, and J. Cunningham, 'Past, Present, and Future Challenges of the Marine Vessel's Electrical Power System', *IEEE Trans. Transp. Electrification*, vol. 2, no. 4, pp. 522–537, Dec. 2016, doi: 10.1109/TTE.2016.2552720.

[7] S. Castellan, R. Menis, A. Tessarolo, F. Luise, and T. Mazzuca, 'A review of power electronics equipment for all-electric ship MVDC power systems', *Int. J. Electr. Power Energy Syst.*, vol. 96, pp. 306–323, Mar. 2018, doi: 10.1016/j.ijepes.2017.09.040.

[8] A. Salem and M. Narimani, 'A Review on Multiphase Drives for Automotive Traction Applications', *IEEE Trans. Transp. Electrification*, vol. 5, no. 4, pp. 1329–1348, Dec. 2019, doi: 10.1109/TTE.2019.2956355.

[9] Z. Zhou, M. Benbouzid, J. Frédéric Charpentier, F. Scuiller, and T. Tang, 'A review of energy storage technologies for marine current energy systems', *Renew. Sustain. Energy Rev.*, vol. 18, pp. 390–400, Feb. 2013, doi: 10.1016/j.rser.2012.10.006.

[10] I. Zoric, M. Jones, and E. Levi, 'Arbitrary Power Sharing Among Three-Phase Winding Sets of Multiphase Machines', *IEEE Trans. Ind. Electron.*, vol. 65, no. 2, pp. 1128–1139, Feb. 2018, doi: 10.1109/TIE.2017.2733468.

[11] J. Carlton, *Marine Propellers and Propulsion, Second Edition*. Butterworth-Heinemann, 2012.

[12] G. Abad, Ed., *Power Electronics and Electric Drives for Traction Applications*, 1 edition. Wiley, 2016.

[13] DAMEN, 'Electric Tug Boat: Design, Construction, Sale'. Accessed: Aug. 04, 2024. [Online]. Available: https://www.damen.com/vessels/tugs/electric-tugs?view=models

[14] ZEETUG, 'First in the World | Zero Emission Clean Operation'. Accessed: Aug. 04, 2024. [Online]. Available: https://www.zeetug.com